A Brillouin light scattering study of the elastic properties of $In_{0.5}Ga_{0.5}As/InP$ superlattices grown by chemical beam epitaxy

1996 J. Phys.: Condens. Matter 8 2265

(http://iopscience.iop.org/0953-8984/8/14/004)

J. Phys.: Condens. Matter **8** (1996) 2265–2272. Printed in the UK

A Brillouin light scattering study of the elastic properties of $In_{0.5}Ga_{0.5}As$/InP superlattices grown by chemical beam epitaxy

G Carlotti†, D Fioretto†, L Palmieri†, G Socino†, A Verdini† and C Rigo‡

† Istituto Nazionale per la Fisica della Materia, Unità di Perugia, Dipartimento di Fisica dell'Università, Via Pascoli, 06100 Perugia, Italy
‡ CSELT, Via Reiss Romoli 274, 10148 Torino, Italy

Received 23 October 1995

Abstract. The Brillouin light scattering technique has been exploited for investigating the elastic properties of $In_xGa_{1-x}As$/InP superlattices, with $x = 0.5$ and a total thickness of several hundreds of nanometres. These superlattices have been grown by chemical beam epitaxy and are close to being lattice matched to the InP substrates. The frequency position in the Brillouin spectra of the Rayleigh surface wave, and of the transverse and longitudinal thresholds for two different propagation geometries, enabled us to determine the three effective elastic constants of the superlattices. A comparison between these experimental values and those expected from calculation based on the properties of InP and InGaAs single films shows that interface effects do not play any significant role in modifying the elastic properties of InGaAs/InP heterostructures.

1. Introduction

Although the elastic properties of binary III–V semiconductor compounds have been extensively studied in the recent past, very few experimental data are currently available regarding the elastic constants of ternary alloys [1]. These latter materials are extensively exploited in the technology of optoelectronics devices, in the form of epitaxial thin films and superlattices. Measuring the whole set of elastic constants of this kind of artificially grown heterostructure, characterized by a reduced dimensionality, is out of the reach of conventional techniques and ultrasonics methods [2]. In this respect, however, surface Brillouin scattering (SBS) has recently proved to be a powerful non-destructive tool for the elastic characterization of thin films and multilayers [3]. In Brillouin light scattering experiments a beam of monochromatic light is focused on the surface of the specimen and the light scattered within a solid angle is frequency analysed in order to map out its spectrum in the GHz range. Because of the conservation of momentum in this photon–phonon interaction, the phonons revealed have wavelengths comparable with that of light, i.e. much larger than both the interatomic distances and the multilayer periodicity, so the medium can be described within the elastic continuum approximation. The power spectrum of the interacting phonons is mapped out from the frequency analysis of the light scattered within a solid angle, by means of a multipass Fabry–Perot interferometer [3].

In previous SBS investigations of epitaxial thin films and superlattices it was shown that a detailed study of the angular dispersion of the Rayleigh wave velocity on the surface plane can yield useful information on the elastic properties [4, 5]. In some specific cases,

0953-8984/96/142265+08$19.50

this procedure has been used for determining the whole set of elastic constants, but this led to rather large errors, especially regarding the value of the elastic constant c_{12} [6]. Very recently, Krieger *et al* used near-infrared Brillouin scattering from bulk waves for determining the elastic constants of the AlGaAs system [7], while Hassine *et al* investigated the acoustic and optical properties of GaInP films with a wide band gap, by studying the scattering of light with different wavelengths from bulk acoustic phonons [8].

In this paper we report on the measurement of the effective elastic constants of three $In_{0.5}Ga_{0.5}As$/InP superlattices, which are rather close to being lattice matched ($\Delta a/a \simeq 0.2\%$), by careful analysis of the surface phonon spectrum obtained via SBS. The whole set of independent elastic constants could be determined by measuring the frequency position of both the transverse and the longitudinal thresholds, in addition to that of the Rayleigh wave peak. In order to give a meaningful interpretation of the experimental results, we have also taken measurements on the single films of the two constituent materials, i.e. InGaAs and InP. This permitted us to compare the constants of the superlattices with those expected from calculations based on the elastic constants of the two constituents. The results obtained are discussed in the light of the theoretical models proposed in the past for explaining the anomalous elastic behaviour observed in both metallic and semiconductor multilayers [9, 10].

2. Sample preparation and characterization

The specimens were grown by chemical beam epitaxy (CBE) using a standard diffusion-pumped VG-80H MBE, connected to a pressure-controlled gas system which has been extensively described in previous papers [11, 12]. Three InGaAs/InP superlattices were prepared on InP substrates, with different thicknesses of the constitutive layers, as reported in table 1. In addition to the three superlattices, two single films of InP and of InGaAs, about 1 μm thick, were grown. The structural properties of all the above heterostructures were analysed via high-resolution x-ray diffraction experiments, using a Philips five-crystal diffractometer. This has shown that the specimens exhibit a high crystal quality, with the interfaces extending over 2–3 atomic planes. The thicknesses of the constitutive layers, the interatomic distances and the stoichiometric composition have been found to agree very well with the nominal ones. The mass density ρ of the superlattices, which is reported in the last column of table 1, has been calculated from the values of the molecular weight and of the elementary cell volume of each material.

3. Measurement of the elastic constants

In the elastic continuum approximation the superlattices analysed here can be modelled as effective media belonging to the tetragonal symmetry group with six independent elastic constants. The values of these constants can be calculated from those of the two constituent materials of cubic symmetry, by imposing the continuity of stress and strain across the interfaces [13]. Following this procedure, however, it turns out that

$$\frac{c_{11}-c_{33}}{c_{11}} \simeq 0.15\% \qquad \frac{c_{12}-c_{13}}{c_{12}} \simeq 0.20\% \qquad \frac{c_{44}-c_{66}}{c_{44}} \simeq 0.15\%.$$

These differences are much lower than the experimental errors of our SBS measurements, so the tetragonal distortion can be assumed to be negligible and the superlattices adequately described as cubic effective media, with only three independent effective elastic constants, namely c_{11}, c_{12}, and c_{44}.

Table 1. Characteristic parameters of the three superlattices and of the two single films investigated here: d_{InP} and d_{InGaAs} are the sublayer thicknesses, p the periodicity, N the total numbers of bilayers, h the total thickness and ρ the mass density.

Specimen	d_{InGaAs} (nm)	d_{InP} (nm)	p (nm)	N	h (nm)	ρ (kg m^{-3})
QW347	3.0	5.5	8.5	59	501.5	5050
QW401	5.7	8.0	13.7	66	904.2	5097
QW411	1.3	1.8	3.1	65	201.5	5099
InP	—	—	—	—	1000	4787
InGaAs	—	—	—	—	680	5531

Measurement of these constants can be performed by a careful analysis of the surface phonon spectrum obtained via SBS. In fact, since the materials investigated here are opaque to the green light used in the experiments, the main mechanism of interaction between incoming photons and phonons is the corrugation of the free surface. Consequently, the efficiency of scattering from surface excitations is enhanced, while bulk excitations present a broadened line shape [14].

Figure 1 shows the component of the surface phonon power spectrum orthogonal to the free surface, for a fixed value of $Q_{\parallel}$ directed along the two main directions [100] and [110]. It can be seen that there is a discrete mode, the Rayleigh wave (RW), at frequency f_{RW}, and a continuum of modes extending to higher frequencies [15]. The continuum of modes presents two dips at the frequencies f_{TT} and f_{LT}, which correspond to the so-called *transverse threshold* (TT) and *longitudinal threshold* (LT), respectively [15]. Since the component $Q_{\parallel}$ of the phonon wavevector is fixed by the experimental interaction geometry, it follows that one can associate the velocities

$$V_{\mathrm{RW}} = 2\pi f_{\mathrm{RW}}/Q_{\parallel} \qquad V_{\mathrm{TT}} = 2\pi f_{\mathrm{TT}}/Q_{\parallel} \qquad V_{\mathrm{LT}} = 2\pi f_{\mathrm{LT}}/Q_{\parallel}$$

with the RW, the TT and the LT, respectively. Some of these velocities are linked to the elastic constants of the medium by rather simple equations, which we present in the following. As far as the Rayleigh wave is concerned [1], for $Q_{\parallel}$ along [100] one has

$$c_{11}\left(V_{\mathrm{RW}}^2 - \frac{c_{44}}{\rho}\right)\left(V_{\mathrm{RW}}^2 - \frac{c_{11}}{\rho} + \frac{c_{12}^2}{c_{11}\rho}\right) - c_{44}V_{\mathrm{RW}}^4\left(V_{\mathrm{RW}}^2 - \frac{c_{11}}{\rho}\right) = 0 \qquad (1)$$

while for $Q_{\parallel}$ along [110]:

$$c_{11}\left(V_{\mathrm{RW}}^2 - \frac{c_{44}}{\rho}\right)\left(V_{\mathrm{RW}}^2 - \frac{c_{11}+c_{12}+2c_{44}}{2\rho} + \frac{c_{12}^2}{c_{11}\rho}\right)^2 - c_{44}V_{\mathrm{RW}}^4\left(V_{\mathrm{RW}}^2 - \frac{c_{11}+c_{12}+2c_{44}}{2\rho}\right) = 0. \qquad (2)$$

As for V_{LT}, it corresponds to the velocity of a longitudinal bulk wave travelling parallel to the surface, so for $Q_{\parallel}$ along [100]

$$V_{\mathrm{LT}} = \sqrt{\frac{c_{11}}{\rho}} \qquad (3)$$

and for $Q_{\parallel}$ along [110]

$$V_{\mathrm{LT}} = \sqrt{\frac{c_{11}+c_{12}+2c_{44}}{2\rho}}. \qquad (4)$$

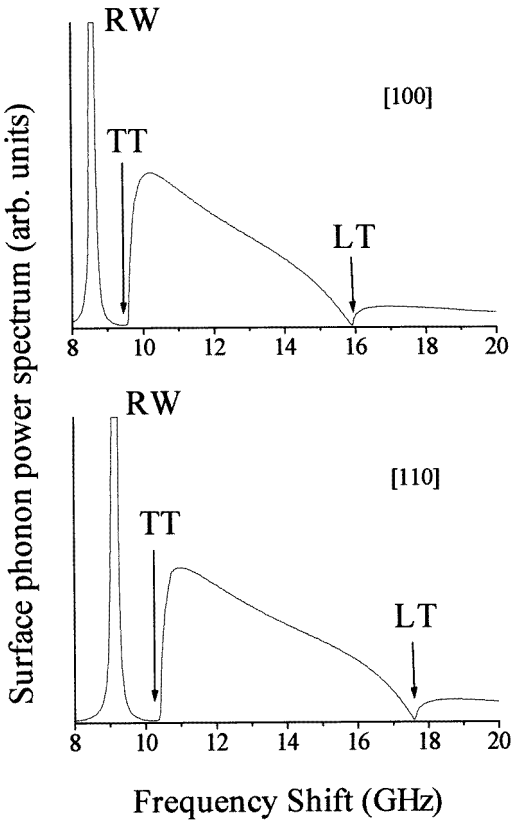

Figure 1. Calculated perpendicular components of the surface phonon power spectra for a value of $Q_{\parallel}$, corresponding to an angle of incidence $\theta = 67.5^{\circ}$. $Q_{\parallel}$ is directed along [100] (upper spectrum) and along [110] (lower spectrum). The peak associated with the Rayleigh wave (RW) and the dips corresponding to the transverse thresholds (TT) and to the longitudinal thresholds (LT) are indicated.

As for V_{TT}, because of the shape of the slowness curve on the sagittal plane [17], it corresponds to the velocity of a bulk shear wave with total wavevector tilted inside the medium at an angle of about 24° from the free surface, and can be related to the elastic constants only through numerical calculations.

In order to visualize the contribution of each elastic constant to the above velocities, we have calculated the relative change of each velocity corresponding to a 1% variation of each constant. The results of this calculation for the specimen QW347 are reported in figure 2. It turns out that $V_{RW}[110]$ and $V_{TT}[110]$ exhibit a similar dependence on the three elastic constants, so knowledge of either of these velocities will yield the same kind of information. On the other hand, determining $V_{LT}[100]$ and $V_{LT}[110]$ provides a large amount of information, because the former depends selectively on c_{11} [18], while the latter is influenced by c_{12} with an opposite sign with respect to all of the other velocities. This is very important as regards determining the three independent constants by a best-fit procedure and permits one to overcome the difficulties of isolating c_{11} and c_{12} experienced in different methods used in the past [6].

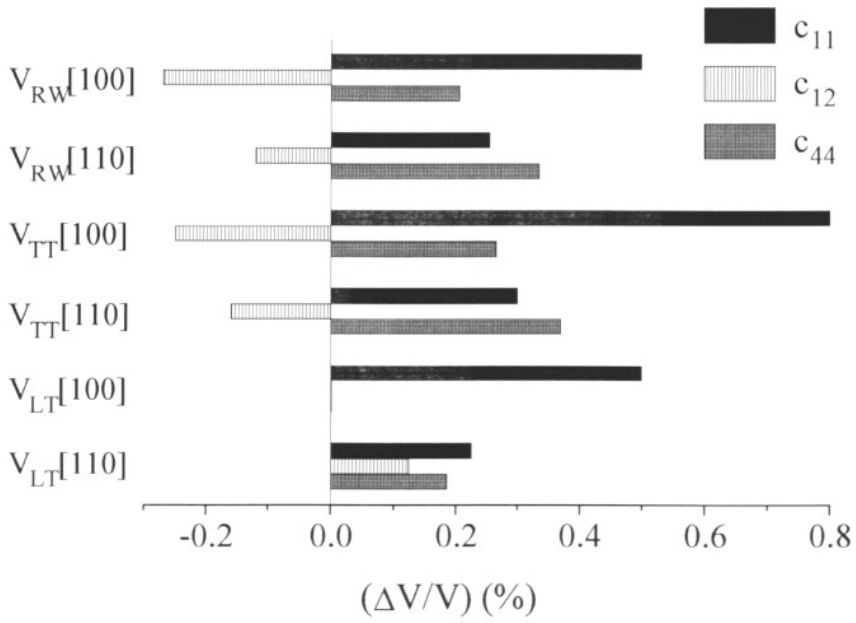

Figure 2. Relative changes of the phase velocities corresponding to the RW, the TT and the LT, separately produced by a 1% increase of each elastic constant. Propagation along both [100] and [110] is considered.

4. Experimental details, results and discussion

Brillouin scattering measurements were performed in air, at room temperature, using a 200 mW p-polarized light beam (a single mode of the 514.5 nm line of an Ar^+ laser). The incident light was focused onto the surface of the specimen and the backscattered light collected by a lens with f-number 2 and focal length 50 mm. The frequency analysis was performed using a Sandercock-type, $3+3$ pass, tandem Fabry–Perot interferometer [3, 19] characterized by a fineness of about 100 and a contrast ratio higher than 5×10^{10}; the sampling time per spectrum was typically three hours. Brillouin spectra were taken in the backscattering interaction geometry, with both the incident and scattered light polarized in the plane of incidence. According to the backscattering interaction geometry, the component of the acoustic wavevector parallel to the surface, $Q_\parallel$, is linked to the optical wavenumber k_i of the incident light by the relationship

$$Q_\parallel = 2k_i \sin\theta \tag{5}$$

with θ the angle of incidence.

Measurements were taken at an angle of incidence of 67.5°, corresponding to an acoustic wavelength of about 278 nm. This value is lower than (or comparable to, in one case) the total thickness of the films investigated, and numerical calculations show that the phase velocities of the waves revealed differ from those of the semi-infinite film material by less than 0.1%. Therefore the influence of the substrate can be assumed to be a negligible effect.

Figure 3 shows typical Brillouin spectra from the QW411 specimen, for propagation along both [100] and [110]. The peak corresponding to the Rayleigh surface wave and the dips associated with the longitudinal and transverse thresholds are clearly seen. In

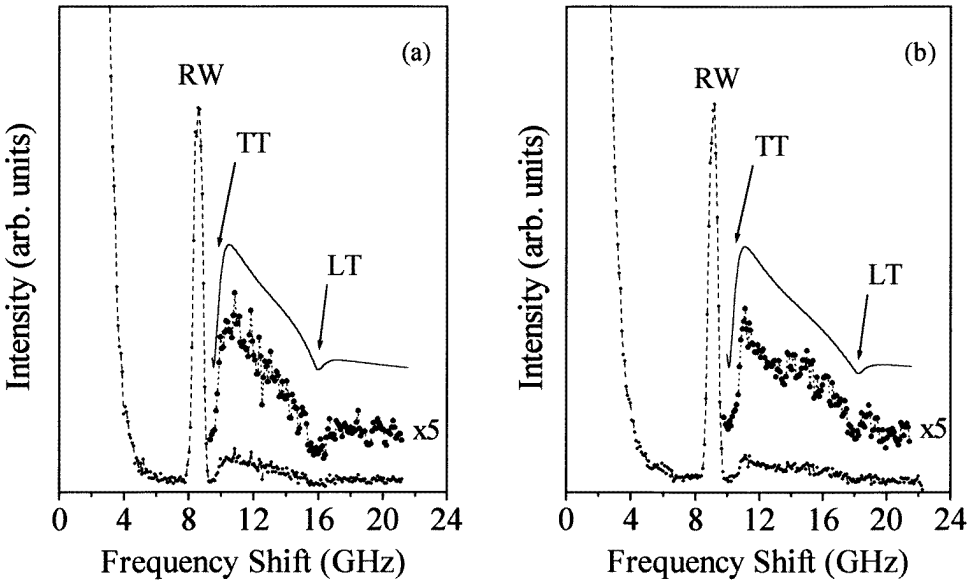

Figure 3. Experimental Brillouin spectra (dots) taken from the specimen QW411 with $Q_{\parallel}$ along [100] (a) and along [110] (b), for an angle of incidence $\theta = 67.5^{\circ}$. The solid lines correspond to the calculated perpendicular components of the surface phonon power spectrum, convoluted with a Gaussian function of width 0.6 GHz (the instrumental resolution).

Table 2. Elastic constants of the three InGaAs/InP superlattices determined experimentally. The values calculated from the experimental elastic constants of the two constituent materials, given in table 3, are also reported.

Specimen		c_{11} (GPa)	c_{12} (GPa)	c_{44} (GPa)
QW347	Experimental	100 ± 2	54.3 ± 1.5	45.2 ± 1.8
	Calculated	100.1	54.7	45.3
QW401	Experimental	100 ± 2	56.1 ± 1.5	45.5 ± 1.8
	Calculated	99.9	54.4	45.5
QW411	Experimental	100 ± 2	54.7 ± 1.5	45.4 ± 1.8
	Calculated	99.9	54.4	45.5

order to reduce the uncertainty in the evaluation of the frequency position of the two thresholds, a direct comparison between the calculated phonon power spectrum (solid line) and the measured Brillouin spectrum (dots) has been performed. Use of a Gauss–Newton iterative best-fit procedure for fitting the calculated RW, TT and LT phase velocities to the experimental ones, for propagation along both [100] and [110], enabled us to determine the three effective elastic constants of the InGaAs/InP superlattices analysed. The results obtained are summarized in table 2. The errors reported for each constant have been evaluated from the uncertainty in the measured velocities.

In order to give a meaningful interpretation of the values obtained for the constants of the superlattices, we have also taken measurements on the two single films of the constituent materials, i.e. InP and InGaAs. Table 3 shows a comparison between the values of the elastic

Table 3. Elastic constants of InGaAs and InP determined experimentally for the single films analysed in the present work. For comparison the corresponding values of the constants of the bulk materials are also reported.

Specimen		c_{11} (GPa)	c_{12} (GPa)	c_{44} (GPa)
InGaAs	Epitaxial film (this work)	98 ± 2	51.8 ± 1.5	46.9 ± 1.8
	Bulk material ([20])	101.1	49.6	49.5
InP	Epitaxial film (this work)	101 ± 2	56.2 ± 1.5	44.4 ± 1.8
	Bulk material ([1])	101.1	56.1	45.6

constants of these two films determined by the same method as was used for the superlattices, with those derived from the available literature data. A very good agreement between the experimental and the expected values can be seen for InP, while only minor deviations appear for the InGaAs film. We notice that to the best of our knowledge this is the first experimental investigation of the elastic constants of both InGaAs films and InGaAs-based superlattices. Using the values determined experimentally for the single films, we have calculated the constants of the superlattices following the procedure of [13]. For the sake of comparison, these calculated values are listed in table 2, just below the corresponding experimental values. It can be seen that there is a good agreement between the two sets of data for all of the specimens investigated, even if they present differences as regards both the periodicity and the ratio between the thicknesses of the constitutive layers. In particular, the results for the specimens QW401 and QW411, which have different periodicities but are characterized by very close fractions of the constituents ($d_{\mathrm{InP}}/d_{\mathrm{InGaAs}} \simeq 1.4$), do not show any significant difference, and this suggests that interface effects do not play any important role in affecting the elastic constants. This ideal behaviour of the epitaxial InGaAs/InP superlattices investigated here is consistent with previous results on both crystalline [21] and amorphous [22, 23] semiconductor multilayers. Moreover, the absence of anomalous behaviour is consistent with the predictions of most of the models proposed for explaining the elastic anomalies observed in the past for metallic superlattices. In fact, in this case one can exclude the influence of electron transfer between the different layers [24], because of the non-metallic nature of the constituents. In addition, effects due to coherency strains [25], atomic disorder and grain boundaries [26] cannot operate because of the almost perfect lattice matching between the constituents, and of the high-quality epitaxial nature of the whole structure.

5. Conclusions

The Brillouin light scattering technique has been exploited for studying the elastic properties of three $In_{0.5}Ga_{0.5}As$/InP superlattices epitaxially grown on InP substrates. Measurement of the frequency position in Brillouin spectra of the Rayleigh wave peak and of the dips associated with the transverse and longitudinal thresholds enabled us to achieve a determination of the three independent stiffness constants of each superlattice. A comparison of the experimental values of the elastic constants of the superlattices with those calculated from the elastic properties of the constituent materials has shown that there

is a good agreement between the two sets of values, with no appreciable dependence on the superlattice periodicity. This absence of anomalous elastic behaviour is consistent with the predictions of most of the models proposed to date for explaining the elastic anomalies observed in metallic superlattices.

Acknowledgments

The authors are grateful to Professor L Verdini for helpful discussions and contributions to this research, Dr V Alexandrov for his assistance in the calculation of the surface phonon spectrum, and the Istituto Nazionale per la Fisica della Materia for partial financial support.

References

[1] Adachi S 1992 *Physical Properties of V–III Semiconductor Compounds* (New York: Wiley) pp 17–47
[2] See, for instance,
Coufal H, Meyer K, Grygier R K, de Vries M, Jenrich D and Hess P 1994 *Appl. Phys.* A **59** 83
[3] Nizzoli F and Sandercock J R 1990 *Dynamical Properties of Solids* vol 6, ed G K Horton and A A Maradudin (Amsterdam: North-Holland) p 307
[4] Zuk J, Kiefte H and Clouter M J 1992 *J. Appl. Phys.* **72** 3504
[5] Sapriel J, Michel J C, Toledano J C, Vacher R, Kervarec J and Regreny A 1983 *Phys. Rev.* B **28** 2007
[6] Elminger M W, Henz J, von Kanel H, Ospelt M and Wachter P 1989 *Surf. Interface Anal.* **14** 18
Mendik M, Ospelt M, von Kanel H and Wachter P 1991 *Appl. Surf. Sci.* **50** 303
[7] Krieger M, Sigg H, Herres N, Bachem K and Kohler K 1995 *Appl. Phys. Lett.* **66** 682
[8] Hassine A, Sapriel J, Le Berre P, Legay P, Alexandre F and Post G 1995 *J. Appl. Phys.* **77** 6569
[9] Grimsditch M 1989 *Light Scattering in Solids V* ed M Cardona and G Guntherodt (Berlin: Springer) p 285
[10] Shen Q, Zhang S Y, Wang Z C, Lu Z N and Yu J 1989 *Phys. Rev.* B **39** 11 016
[11] Rigo C, Antolini A, Cacciatore C, Coriasso C, Lazzarini L and Salviati G 1994 *J. Cryst. Growth* **136** 293
[12] Genova F, Antolini A, Francesio L, Gastaldi L, Lamberti C, Papuzza C and Rigo C 1992 *J. Cryst. Growth* **120** 333
[13] Grimsditch M 1985 *Phys. Rev.* B **31** 6818
[14] Loudon R and Sandercock J 1980 *J. Phys. C: Solid State Phys.* **13** 2609
[15] Marvin A M, Bortolani V, Nizzoli F and Santoro G 1980 *J. Phys. C: Solid State Phys.* **13** 1607
[16] Zirngiebl E and Guntherodt G 1991 *Light Scattering in Solids VI* ed M Cardona and G Guntherodt (Berlin: Springer) pp 255–9
[17] Auld B A 1973 *Acoustic Fields and Waves in Solids* (New York: Wiley)
[18] Carlotti G, Fioretto D, Giovannini L, Socino G, Pelosin V and Rodmacq B 1992 *Solid State Commun.* **81** 487
[19] A schematic diagram of the experimental apparatus can be found in
Carlotti G, Fioretto D, Socino G, Verdini L and Pelosin V 1993 *J. Appl. Phys.* **73** 3028
[20] Moise T S, Guido L J and Barker R C 1993 *Phys. Rev.* B **47** 6758
[21] Grimsditch M, Bhadra R, Schuller I K, Chambers F and Devane G 1990 *Phys. Rev.* B **42** 2923
[22] Xia Hua, Carlotti G, Socino G, Chen K J, Zhang Wei, Li Z F and Zhang X K 1994 *J. Appl. Phys.* **75** 475
[23] Carlotti G, Socino G, Hua Xia, Chen K J, Li Z F, Wei Zhang and Zhang X K 1994 *J. Phys.: Condens. Matter* **6** 6095
[24] Hubberman M L and Grimsditch M 1989 *Phys. Rev. Lett.* **62** 1403
[25] Jankowsky A F 1988 *J. Phys. F: Met. Phys.* **18** 413
[26] Wolf D and Lutsko J F 1989 *J. Appl. Phys.* **66** 1961